RF DESIGN OF A WAVEGUIDE HOM-DAMPING 1.3 GHz SUPERCONDUCTING CAVITY PROTOTYPE

W. Z. Chen[1,2], X. W. Wu[*,2], Z. T. Zhao[†,3], X. H. Guo[1]
[1]ShanghaiTech University, Shanghai, China
[2]Zhangjiang Laboratory, Shanghai China
[3]Shanghai Institute of Applied Physics, Chinese Academy of Sciences, Shanghai China

Abstract

Superconducting radio-frequency (SRF) cavities represent a key technology for modern particle accelerators. In high-current energy recovery linac (ERL) facilities, suppressing higher-order modes (HOMs) is critical to ensure beam stability and minimize additional cryogenic heat loads. This work introduces a waveguide-based scheme to extract and damp harmful HOMs excited by intense beams. A systematic RF design and optimization procedure for this waveguide damping method is presented. By implementing the damping scheme into a single-cell cavity geometry, consistent HOM suppression is achieved while maintaining good properties for the fundamental accelerating mode. The single-cell waveguide HOM-damping cavity, adopting the TESLA shape with an enlarged beam pipe, is currently under fabrication and will be tested in cryogenic experiments.

INTRODUCTION

Energy recovery linac (ERLs) have become a promising solution for modern high-brightness, high-effciency accelerator applications. For high-current ERL operation, the higher-order modes (HOMs) excited by intense beam loads in superconducting radio-frequency (SRF) cavities can lead to beam breakup instability, additional cryogenic heat load, and degraded beam stability [1]. Therefore, effective HOM damping is essential to ensure reliable and stable machine operation.

Various HOM damping concepts have been investigated, such as coaxial couplers, beampipe absorbers, and waveguide dampers. Among these solutions, waveguide-based HOM damping offers broadband damping performance, high power handling capability, and a compact layout, making it a preferred choice for high-current SRF cavities [2, 3].

This paper presents the design and fabrication of a 1.3 GHz single-cell SRF cavity prototype with waveguide HOM damping. The cavity is developed for high-current ERL applications with a nominal beam current of 10 mA. The design focuses on the waveguide HOM damping optimization, fundamental mode leakage, multipacting analysis, and mechanical design. The prototype will be used to validate the waveguide fabrication techniques and support the development of a multi-cell waveguide-damped SRF cavity in the future.

* wuxw@zjlab.ac.cn
† zhaozt@sinap.ac.cn

RF CAVITY DESIGN

For high-current ERL applications, the HOM damping performance is evaluated according to the longitudinal and transverse impedance thresholds derived from beam stability constraints. The longitudinal threshold for monopole modes is determined based on the beam-induced HOM power [4], as expressed in Eq. (1):

$$P = 2 \times I^2 Q_e (R/Q)_{\parallel}. \tag{1}$$

Given the design beam current $I = 10$ mA and a allowable cavity HOM power of 3.6 kW [5], the longitudinal shunt impedance $Q_e(R/Q)_{\parallel}$ should be lower than $3.6 \times 10^7\ \Omega$.

The transverse threshold for dipole modes is obtained from the beam breakup (BBU) threshold current [6] given by Eq. (2):

$$I_{th} \approx \frac{2}{e} \frac{E_0}{Q_e (R/Q)_{\perp} k}, \tag{2}$$

where k denotes the wave number of the dipole mode, and E_0 is the beam energy. For a beam energy of 10 MeV [7], the transverse impedance limit can be deduced from Eq. (2), yielding $Q_e(R/Q)_{\perp} k < 2 \times 10^9\ \Omega/\mathrm{m}$.

Waveguide optimization focuses on four parameters: cross-section, edge blend radius, length, and position. In stage 1, the cross-section and blend radius are optimized by using a 3-cell cavity model, as shown in Fig. 1a, to meet HOM damping and impedance thresholds. The 3-cell model is used because the designed HOM-damping waveguide will be applied to a multi-cell cavity in the future. In stage 2, waveguide length and position are optimized with a single-cell model, as shown in Fig. 1b, to ensure sufficient fundamental-mode attenuation and avoid cavity quench in cryogenic tests. This two-stage optimization achieves strong HOM damping while maintaining stable fundamental-mode performance.

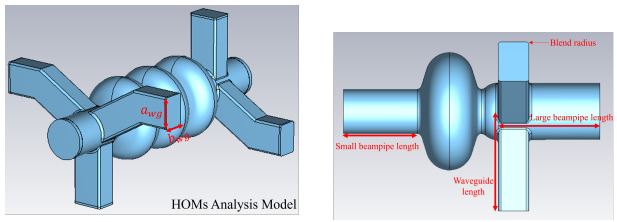

(a) (b)

Figure 1: (a) Model of the 3-cell cavity; (b) Model of the single-cell cavity.

Waveguide Cross-Section and Blend Radius

Waveguide optimization is performed using eigenmode simulation in CST. For clear comparison, waveguide designs with different geometric parameters are summarized and labeled in Table 1. a_{wg} and b_{wg} denote the long and short sides of the waveguide cross-section, respectively. The dimensions correspond to the positions indicated in Fig. 1a.

An initial waveguide size of WR340 [8] (Design 1) was first adopted. However, the large a_{wg} led to structural interference between adjacent waveguides. We therefore reduced a_{wg} to 80 mm (Design 2), with negligible changes to HOM impedance, as illustrated in Fig. 2.

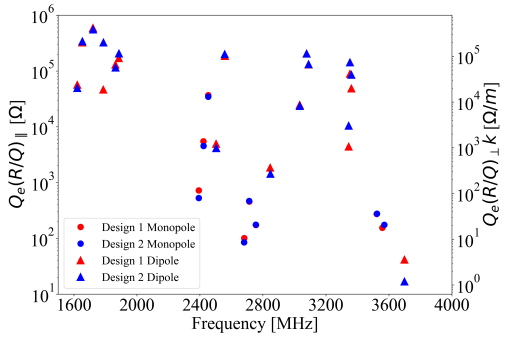

Figure 2: Monopole and dipole mode impedance comparison for designs 1 and 2.

Table 1: Waveguide Cross-Section Dimensions

Design	a_{wg} **(mm)**	b_{wg} **(mm)**
Design 1	86	43
Design 2	80	43
Design 3	80	50
Design 4	80	55

However, several HOMs, such as sextupole modes, are found to have relatively high Q_e in post-processing, which means the cutoff frequency needs to be lowered to properly extract these HOMs.

To further investigate and suppress such high-Q_e HOMs, b_{wg} is selected as the single variable from Design 2 to Design 4, and the corresponding Q_e spectra are compared. The results show that the Q_e of most HOMs decreases significantly with increasing b_{wg}, especially for modes above 2.7 GHz, as shown in Fig. 3.

To further assess the damping performance against the beam stability criteria, the monopole and dipole mode impedances are analyzed across Design 2 to Design 4, as illustrated in Fig. 4. For most dipole mdoes, the transverse impedance $Q_e(R/Q)_\perp k$ decreases evidently as b_{wg} increases. However, the impedance of a small number of modes rises with enlarging b_{wg}, which is unfavorable for overall HOM suppression. For monopole modes, the longitudinal shunt impedance presents a monotonically increasing trend with the growth of b_{wg}. Importantly, the impedance values of all evaluated modes in every design scheme stay well below the aforementioned required threshold. Finally, after a comprehensive trade-off between the undesirable impedance rise

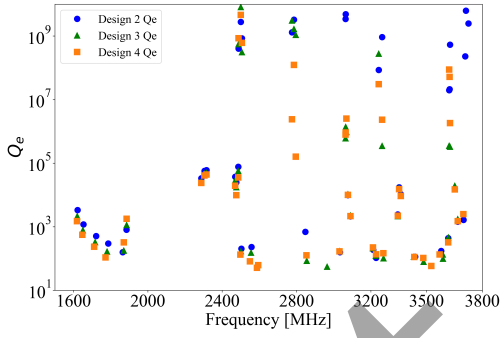

Figure 3: Q_e distribution of Design 2-4.

of partial modes and the effective impedance reduction of dominant dangerous modes, b_{wg} = 55 mm is determined as the optimal dimension, corresponding to Design 3 in this work.

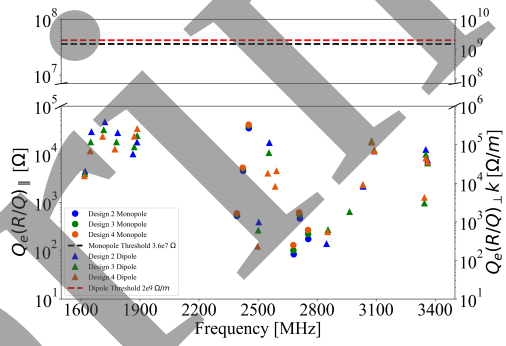

Figure 4: Impedance comparison of monopole and dipole modes in designs 2–4.

After determining the optimal waveguide cross-section, the edge blend radius is further optimized. Sharp structural edges cause severe local electric field concentration and raise the risk of cavity quench during cryogenic RF tests. Parametric analysis of the blend radius is carried out to suppress peak field enhancement while maintaining the optimized HOM damping performance. Blend radii of 5 mm and 10 mm are compared with the unblend configuration. The blend radius is found to have little influence on HOM damping, with negligible variations in mode impedances. Consequently, a blend radius of 5 mm is finally adopted.

Waveguide Length and Position

In this section, the length and position of the waveguide are investigated. The single-cell prototype is mainly used to validate waveguide fabrication techniques, rather than to test HOM damping capability. Therefore, the waveguide ends are sealed with niobium blind plates. The target intrinsic quality factor Q_0 is 1×10^{10}. To limit the Q-drop induced by blind plate losses within 1 % [3], the external quality factor at the waveguide end should satisfy $Q_e > 100Q_0 = 1 \times 10^{12}$. In this optimization, the waveguide position is fixed at the same location determined in the cross-section optimization. Only the waveguide length is varied to find a configuration that satisfies the Q_e criterion. The electrical conductivity of niobium at 50 K is set to $\sigma = 5.6 \times 10^7$ S/m in the CST simulation [9].

As shown in Fig. 5, a waveguide length of 175 mm satisfies the Q_e requirement, and the adopted waveguide position is reasonable and acceptable. Thus, further optimization of the waveguide position is unnecessary.

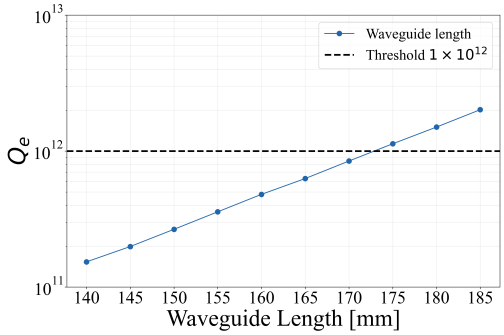

Figure 5: Waveguide length optimization for the single-cell prototype.

Beampipe Length Optimization

For the same concern of fundamental mode leakage, the large and small beampipes also need to be optimized to limit the Q-drop induced by stainless steel flange losses within 1 % [3]. The corresponding requirement is also $Q_e > 1 \times 10^{12}$, and stainless steel with an electrical conductivity of $\sigma = 1.35 \times 10^6$ S/m at room temperature is adopted. Simulation analysis shows that a 170 mm large beampipe and a 130 mm small beampipe can satisfy this criterion.

In the RF vertical test, each beampipe of this single-cell prototype will be equipped with an antenna. Insufficient beampipe length will cause the antenna to couple excessive RF power out of the cavity. Accordingly, two cases are investigated to determine a feasible configuration for the prototype. Case 1 takes the large beampipe as the signal pickup side, while Case 2 adopts the small beampipe for signal pickup. The antenna is required to satisfy a Q_e threshold larger than 1×10^{12}. All calculations are performed using the waveguide port method in CST, and the simulated results are presented in Fig. 6.

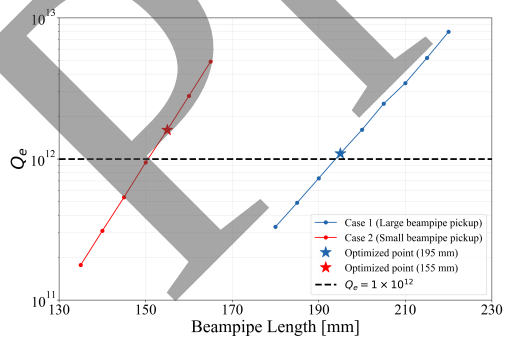

Figure 6: Optimization of beampipe length for antenna signal pickup.

Finally, a 155 mm small beampipe is selected as the signal pickup side in Case 2. Combined with the 170 mm large beampipe mentioned before, this configuration achieves a more balanced beampipe length layout for the single-cell cavity.

MULTIPACTING ANALYSIS

Multipacting (MP) is a resonant electron discharge phenomenon commonly encountered in radiofrequency structures. It arises from the synchronization of emitted electrons with RF fields, as well as electron multiplication upon impact with the structural inner surface [10, 11]. In this section, the connection between the waveguides and the beampipe is included to do the MP analysis.

CST eigenmode and PIC solvers are adopted for the simulation. The simulation covers approximately 40 RF cycles, and the secondary electron yield (SEY) curve of 300 °C baked niobium is implemented in the model. Primary electron sources are placed in the red highlighted regions illustrated in Fig. 7a. The particle growth rate α is obtained by fitting the particle number data [12], as shown in Fig. 7b. The results indicate that multipacting will not occur ($\alpha \leq 0$) with the current waveguide design, so the multipacting risk can be neglected.

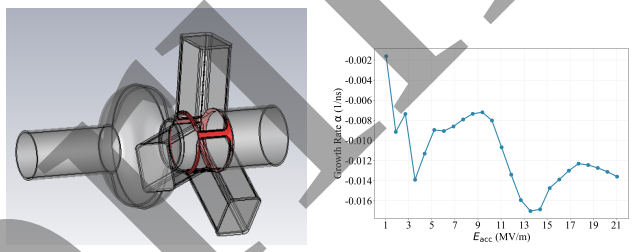

(a) (b)

Figure 7: a) Locations of the particle source; b) Growth rate vs E_{acc} from 1 MV/m to 21 MV/m.

CONCLUSION

A 1.3 GHz CW-mode single-cell SRF cavity with waveguide HOM damping is designed and fabricated for future 3-cell cavity development targeting 10 mA ERL operation. Optimized waveguide geometry, including an 80 mm × 55 mm cross-section, 175 mm length and 5 mm blend radius, meets monopole and dipole damping demands and mitigates local electric field concentration. Beampipe lengths are also optimized to suppress fundamental mode leakage and ensure stable antenna signal pickup. Multipacting simulation verifies no resonance occurs from 1 to 20 MV/m. The prototype has been successfully fabricated, validating waveguide fabrication techniques, and is now ready for surface treatment and cryogenic vertical RF tests.

ACKNOWLEDGEMENTS

This work is supported by Zhangjiang Laboratory.

REFERENCES

[1] L. Merminga, “Energy-Recovery Linacs”, in *Synchrotron Light Sources and Free-Electron Lasers. Accelerator Physics, Instrumentation and Science Applications*, E. Jaeschke, S. Khan, J. R. Schneider, and J. B. Hastings, Eds. Cham, Switerland: Springer, 2015, pp. 1–33. doi:10.1007/978-3-319-04507-8_11-1

[2] F. Marhauser, "Next generation HOM-damping", *Supercond. Sci. Technol.*, vol. 30, no. 6, p. 063002, 2017. doi:10.1088/1361-6668/aa6b8d

[3] A. Tsakanian, A. Vélez, E. Sharples-Milne, and J. Knobloch, "Design of hom damped multi-cell srf cavities for cw operation in high current storage rings", *IEEE Trans. Appl. Supercond.*, vol. 35, no. 4, pp. 1–16, 2025. doi:10.1109/TASC.2025.3554959

[4] M. Liepe, "Conceptual layout of the cavity string of the Cornell ERL main linac cryomodule", in *Proc. SRF'03*, Lübeck/Travemünder, Germany, Sep. 2003, paper MOP33, pp. 115–119.

[5] H.-J. Zheng, J. Gao, and Z.-C. Liu, "Cavity and HOM coupler design for CEPC", *Chin. Phys. C*, vol. 40, no. 5, p. 057001, 2016. doi:10.1088/1674-1137/40/5/057001

[6] A. Neumann *et al.*, "Results and performance simulations of the main linac design for BERLinPro", in *Proc. LINAC'12*, Tel Aviv, Israel, Sep. 2012, paper MOPB067, pp. 333–335.

[7] X. Chen *et al.*, "The design of high-brightness ERL-FEL injector based on VHF electron gun", *Nucl. Instrum. Meth. A*, vol. 1070, p. 170058, 2025. doi:10.1016/j.nima.2024.170058

[8] K. V. D. K. Reddy, M. T. Wara, V. Suneeta, and K. Chandrasekharam, "Design and development of S-band WR-340 waveguide full height to quarter height transitions for satellite testing applications", in *2025 IEEE Space Aerosp. Def. Conf. (SPACE)*, Bangalore, India, Jul. 2025, pp. 1–5. doi:10.1109/SPACE65882.2025.11170525

[9] N. Morton, B. W. James, G. H. Wostenholm, and R. J. Nichols, "The electrical resistivity of niobium and niobium-zirconium alloys", *J. Phys. F: Met. Phys.*, vol. 5, no. 1, p. 85, Jan. 1975. doi:10.1088/0305-4608/5/1/013

[10] H. Padamsee, J. Knobloch, and T. Hays, *RF Superconductivity for Accelerators*. Hoboken, NJ, USA: Wiley, 1998.

[11] R. F. Parodi, "Multipacting", in *Proc. CERN Accel. Sch.: Course RF Accel.*, Ebeltoft, Denmark, Jun. 2010. doi:10.48550/arXiv.1112.2176

[12] G. Romanov, "Simulation of multipacting in HINS accelerating structures with CST particle studio", in *Proc. LINAC'08*, vol. 159, Victoria, BC, Canada, Sep.–Oct. 2008, paper MOP043, pp. 166–168.